Bachelor Thesis

Investigation of the ^{42}K Background in GERDA Phase II Data

Untersuchung des ^{42}K Untergrundes in GERDA Phase II Daten

Mirco Troue

August 7, 2018

Technical University Munich
Department of Physics

E15 Chair for Experimental Physics and Astroparticle Physics

First supervisor:	Prof. Dr. rer. nat. Stefan Schönert
Second supervisor:	Apl. Prof. Dr. rer. nat. habil. Hubert Kroha
Advisors:	Christoph Wiesinger, Tommaso Comellato

Abstract

The GERDA experiment at LNGS searches for neutrinoless double beta decay in ^{76}Ge with a current median sensitivity of $T^{0\nu}_{1/2} = 11 \times 10^{25}\,\mathrm{yr}$ [1]. The high purity germanium detectors are located inside of liquid argon, which contains a small amount of ^{42}Ar, that decays into ^{42}K ions. These ions accumulate on the surface of the detectors, due to high voltage bias. This leads to a background inside the energy range where a neutrinoless double beta decay could happen.

This thesis investigates the amount of background produced by ^{42}K and presents different ways for suppression by studying Run 52 during Phase II commissioning. In this specific run, only two detector strings were equipped with a Nylon Mini Shroud working as a physical barrier for ^{42}K transport to the detectors. The increase in background, compared to a setup where all detector strings are equipped with a Nylon Mini Shroud (NMS), allows for an in situ comparison between Pulse Shape Analysis and the Liquid Argon Instrumentation of GERDA.

Finally, a Background Index of $10.4^{+35.1}_{-9.3}\ \frac{\mathrm{cts}}{\mathrm{keV\,kg\,yr}}$ is obtained and upper limits for the expected ^{42}K suppression with the different methods are acquired. Combined cuts yield a central ^{42}K survival fraction of $\approx 3.3\,\%$.

Zusammenfassung

Das GERDA Experiment am LNGS sucht nach dem neutrinolosem Doppel-Beta-Zerfall in ^{76}Ge mit einer momentanen Sensitivität von $T^{0\nu}_{1/2} = 11 \times 10^{25}\,\mathrm{yr}$ [1]. Die hochreinen Germanium Detektoren befinden sich in flüssigem Argon. Es enthällt einen geringen Anteil ^{42}Ar, welches zu ^{42}K Ionen zerfällt. Diese sammeln sich aufgrund der Hochspannungsversorgung an den Detektoroberflächen an, wo sie zu einem Untergrund innerhalb des Energiebereiches, in welchem ein neutrinoloser Doppel-Beta-Zerfall stattfinden könnte, führen.

Die vorliegende Arbeit untersucht den durch ^{42}K induzierten Untergrund und stellt verschiedene Möglichkeiten zur Unterdrückung vor, indem Run 52 während der Inbetriebnahme von Phase II untersucht wird. In diesem speziellen Run wurden lediglich zwei Detektor Stränge mit einer Nylon Mini Shroud ausgestattet, welcher als physische Barriere für die ^{42}K Ionen dient. Die Verstärkung des Untergrundes, verglichen mit dem Untergrund ohne Verwednung einer Nylon Mini Shroud, erlaubt einen in situ Vergleich zwischen Pulsformanalyse und dem Argon System von GERDA.

Schließlich wird ein Untergundindex von $10.4^{+35.1}_{-9.3}\ \frac{\mathrm{cts}}{\mathrm{keV\,kg\,yr}}$ ermittelt und Obergrenzen für die mittlere ^{42}K Überlebensrate für die einzelnen Methoden bestimmt. Unter Verwendung aller Cuts ergibt sich eine mittlere ^{42}K Überlebensrate von $\approx 3.3\,\%$

Contents

List of Abbreviations

A/E	Amplitude over Energy
BEGe	Broad Energy Germanium
BI	Background Index
DEP	Double Escape Peak
FEP	Full Energy Peak
FWHM	Full width at half maximum
GERDA	Germanium Detector Array
LAr	Liquid Argon
LNGS	Laboratori Nazionali del Gran Sasso
MS	Mini Shroud
MSE	Multi Site Event
NMS	Nylon Mini Shroud
PMNS	Pontecorvo–Maki–Nakagawa–Sakata
PMT	Photomultiplier tube
PSD	Pulse Shape Discrimination
ROI	Region Of Interest
SEP	Single Escape Peak
SiPM	Silicon Photomultiplier
SSE	Single Site Event
TP	Test Pulse
TPB	1,1,4,4-tetraphenyl-1,3-butadiene
WLS	Wave Lenght Shifting

1. Introduction

1.1. Neutrinos

The neutrino was postulated in 1930 by Wolfgang Pauli as a solution to the continuous energy spectrum in β^- decay [2]. However, because of its weakly interacting nature, it was not observed until 26 years later when experiments performed by Cowan and Reines were able to detect anti-electron neutrinos via inverse beta decay using a nuclear reactor as a neutrino source [3].

A member of the second generation, the muon neutrino, was found in 1962 by Jack Steinberger, Melvin Schwartz and Leon Max Lederman [4]. After the observation of the tau lepton, the third generation of neutrinos was expected and found with the Direct Observation of the Nu Tau (DONUT) experiment at Fermilab in 2000 - the tau neutrino [5].

These three neutrinos and their antiparticles are described in the standard model of particle physics. It states that all neutrinos are massless. All neutrinos and their antiparticles are fermions with spin $1/2$ and no charge.

Although the standard model differentiates between those two, neutrinos could be their own antiparticles. Fermions which are not identical to their antiparticles are called Dirac fermions. If the neutrino would be its own antipartner it would be a Majorana fermion, concluding that the required conservation of all quantum numbers would lead to a violation of the lepton number. [6]

Most modern theoretical approaches handle neutrinos as Majorana fermions.

1.2. Neutrino Oscillation

The weak and the mass eigenstates for neutrinos are not identical. First hypothetical approaches for neutrino mixing were done by Bruno Pontecorvo in 1957 [7]. Five years later, Maki, Nakagawa and Sakata introduced a theoretical description [8]. The unitary Pontecorvo–Maki–Nakagawa–Sakata (PMNS) matrix describes the neutrino mixing

$$\begin{pmatrix} \nu_e \\ \nu_\mu \\ \nu_\tau \end{pmatrix} = \begin{pmatrix} U_{e1} & U_{e2} & U_{e3} \\ U_{\mu 1} & U_{\mu 2} & U_{\mu 3} \\ U_{\tau 1} & U_{\tau 2} & U_{\tau 3} \end{pmatrix} \begin{pmatrix} \nu_1 \\ \nu_2 \\ \nu_3 \end{pmatrix}. \tag{1.1}$$

The left vector describes a neutrino state in the flavor basis. The far right vector describes the mass basis. ν_1, ν_2 and ν_3 have well defined masses. [9]

The first hint for oscillating neutrinos was the solar neutrino flux. Fusion inside our sun generates electron neutrinos.

The detected electron neutrino flux at the earth's surface was significantly lower of what was expected from solar models. In 2001, the Sudbury Neutrino Observatory was able to detect flux of all flavors in solar neutrinos and therefore solved the solar neutrino puzzle [10]. At the same time, the Super-Kamiokande Collaboration measured oscillating atmospheric neutrinos [11].

These experimental discoveries were rewarded with a Nobel Prize "for the discovery of neutrino oscillations, which shows that neutrinos have mass" [12] in 2015. Various experiments using either solar, atmospheric, reactor or accelerator neutrinos followed and were able to constrain the parameters in the PMNS matrix. [9]

1.3. Double Beta Decay

Double Beta ($\beta\beta$) Decay is a weak second-order process which occurs if a single beta decay is forbidden, mostly by energy conservation. The two-neutrino double beta ($2\nu\beta\beta$) decay can be seen as a simultaneous occurrence of two beta decays. Two neutrons are transforming into two protons, two electrons and two anti-electron neutrinos, as shown in figure 1.1.

The mass of an isotope can be expressed as

$$m = Zm_P + Nm_N - \frac{E_B}{c^2}\,, \tag{1.2}$$

with Z the number of protons and N the number of neutrons inside the nucleus. The empirical Weizsäcker mass formula describes the mass

$$m(Z, A = const.) \propto \alpha Z + \beta Z^2 + \begin{cases} -a_P A^{-1/2} & Z,\ N \text{ even} \\ 0 & A \text{ odd} \\ +a_P A^{-1/2} & Z,\ N \text{ odd} \end{cases} \tag{1.3}$$

for constant A. [13]

All $\beta\beta$ decaying isotopes feature even-even nuclei and decay into even-even daughter nuclei changing their number of protons by two. The decay of interest is the double beta decay of ^{76}Ge:

$$^{76}_{32}\mathrm{Ge} \rightarrow {}^{76}_{34}\mathrm{Se} + 2e^- + 2\bar{\nu_e} \tag{1.4}$$

The corresponding Q-value is $(2039.061 \pm 0.007)\,\mathrm{keV}$ [14].

1.4. Neutrinoless Double Beta Decay

Assuming neutrinos are massive Majorana fermions, a second type of $\beta\beta$ decay is possible of which one channel is shown in figure 1.1. Neutrinoless double beta ($0\nu\beta\beta$) decay is a theoretical process in which two electrons and no neutrinos are produced.

The two emitted electrons carry the whole energy, if the rather small recoil of the nucleus is neglected. Thus a identification of two electrons with a total energy of around 2039 keV would indicate a $0\nu\beta\beta$ event.

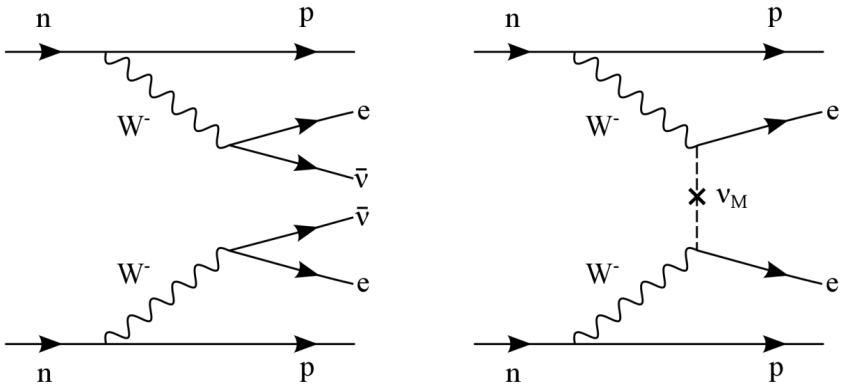

Figure 1.1.: Feynman diagrams of double beta decay (left: $2\nu\beta\beta$, right: $0\nu\beta\beta$ via exchange of a massive Majorana neutrino) from [15]

Decay Rates

Assuming light Majorana neutrino exchange, the total decay rate for $0\nu\beta\beta$ decay is

$$\frac{\Gamma^{0\nu}}{\ln 2} = \frac{1}{T^{0\nu}_{1/2}} = \left\langle m^2_{\nu_e} \right\rangle \left| M^{0\nu} \right|^2 G^{0\nu} \tag{1.5}$$

with the nuclear matrix element $M^{0\nu}$, the phase space factor $G^{0\nu}$ and the effective Majorana mass

$$\left\langle m^2_{\nu_e} \right\rangle = \left| \sum_i U^2_{ei} m_i \right|,$$

with the matrix elements U_{ei} from the PMNS matrix [16].

One task of Germanium Detector Array (GERDA) and similar experiments is to find $0\nu\beta\beta$ decay. If this lepton number violating process were found, the Majorana character of the neutrino would be established. The corresponding effective neutrino mass would allow constraints on the Majorana phases in the PMNS matrix and the general mass scale for all generations of neutrinos.

2. The Germanium Detector Array

GERDA is one of the experiments at the INFN Laboratori Nazionali del Gran Sasso (LNGS) in Gran Sasso d'Italia near L'Aquila. It is located underground under rock with 3500 m of water equivalent to eliminate cosmic rays and reduce the muon flux down to $\approx 1.25 \frac{1}{\mathrm{m}^2\,\mathrm{h}}$. [17]

2.1. Setup

The general setup of GERDA is shown in figure 2.1. A temperature stabilized clean room is used. It is located under a muon veto made out of plastic scintillator and contains a lock for maintenance and assembly of the detectors and the Liquid Argon (LAr) instrumentation inside a glove box. The detector array is lowered inside a cryostat with 64 m^3 LAr and surrounded by a 590 m^3 water tank with 66 Photomultiplier tubes (PMTs) used as a Cherenkov veto. [17]

The heart of the setup are the High Purity Germanium (HPGe) detectors and the LAr veto system, which will be described hereafter. The break after data taking of Phase I was used to improve the setup. All components with a red label in figure 2.1 were modified for Phase II.

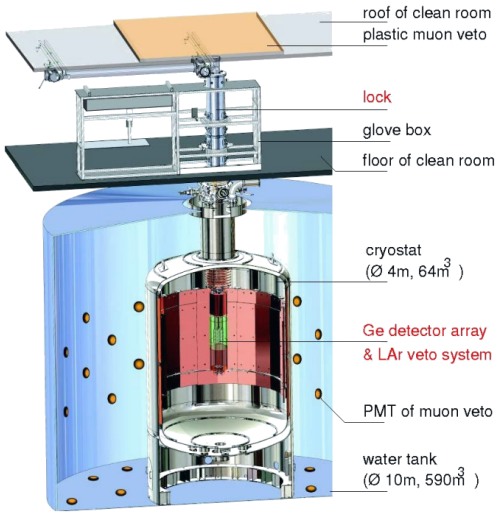

Figure 2.1.: GERDA setup (Phase II components marked in red)

2.1.1. Germanium Detectors

Two types of germanium detectors are used in GERDA: Broad Energy Germanium (BEGe) ones and semi-coaxial ones. BEGes feature an ^{76}Ge enrichment fraction of 87.8 %, semi-coaxial ones vary from 85.5 % to 88.3 %. Both types follow the same principle for detection of radiation with semiconductors. A single detector can be seen as a reverse-biased diode consisting of germanium with a p^+-p-n^+-junction. Ionizing radiation is able to generate electron hole pairs inside the germanium. To measure the energy of the radiation, the charges have to be separated and collected by applying a

bias voltage to the electrodes of the detector. Hence, the depletion zone of the diode, in which recombination of electrons and holes leads to no free charge carriers, is enlarged. It forms the active region of the detector. The read-out of the separated charges is done at the highly conductive p^+ electrode. [17]

Generally speaking, the semi-coaxial detectors have a higher mass than the utilized BEGes. The total mass in Phase II of this detector type was 15.6 kg. BEGes have a smaller p^+ electrode, a lower capacity and therefore a better energy resolution. Furthermore, Pulse Shape Discrimination (PSD) is easier and yields better results [18]. A total BEGe mass of 20 kg was used.

A schematic of the two different types can be found in figure 2.2.

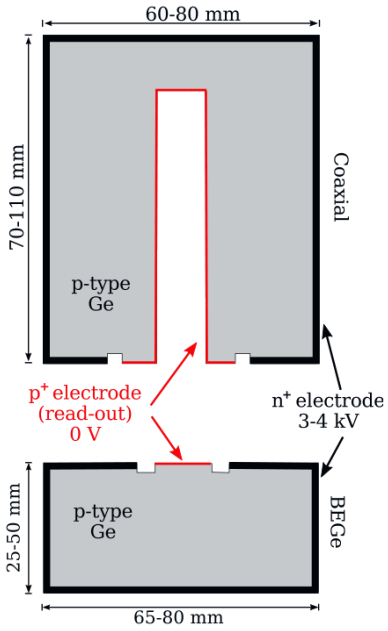

Figure 2.2.: Coaxial HPGe detector and BEGe detector schematics from [19]

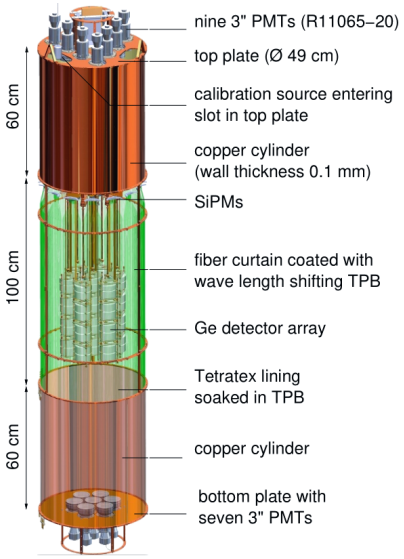

Figure 2.3.: LAr veto system with detector array

2.1.2. LAr Veto

The LAr veto system detects scintillation light of Ar in the volume around the detector array. Whenever energy deposition inside a germanium detector coincides with energy deposition inside the LAr, the event gets rejected. Hence, mainly γ background can be suppressed. The effect on other decays e.g. ^{42}K will be discussed in chapter 5.3.

It consists of a combination of PMTs and a fiber curtain with Silicon Photomultiplier (SiPM) read-out, as shown in figure 2.3. The PMTs are mounted on copper plates, nine at the top of the volume and seven at the bottom. The Tetratex© Polytetrafluorethylen lining inside the copper cylinders above and below the PMTs is covered with 1,1,4,4-tetraphenyl-1,3-butadiene (TPB) for Wave Lenght Shifting (WLS) of the scintillation

light from 128 nm to 425 nm. This is necessary for the light detection because PMTs and also SiPMs have their maximum quantum efficiency in the visible spectrum.

The WLS fibers are read out at each end by the SiPMs at the top of the detector array. TPB is used at the fiber surface again. [17]

2.2. Present Results

First measurements with GERDA were taken in November 2011, the beginning of Phase I. Data was collected until May 2013 leading to a total exposure of 21.6 kg yr in this time. Analysis was able to determine an lower limit for $0\nu\beta\beta$ decay of $T^{0\nu}_{1/2} > 2.1 \times 10^{25}$ yr at a median sensitivity of $T^{0\nu}_{1/2} = 2.4 \times 10^{25}$ yr [20]. Furthermore, the ^{76}Ge $2\nu\beta\beta$ half-life was determined to be $T^{2\nu}_{1/2} = (1.926 \pm 0.094) \times 10^{21}$ yr [21].

After Phase I the setup was changed. New detectors and a new LAr veto were implemented. Phase II was started in December 2015 and data was taken until April 2018 yielding an exposure of 58.9 kg yr in Phase II and a combined exposure with Phase I data of 82.4 kg yr. The analysis resulted in a half life of $T^{0\nu}_{1/2} > 9 \times 10^{25}$ yr with a median sensitivity of $T^{0\nu}_{1/2} = 11 \times 10^{25}$ yr in the Frequentist analysis. This corresponds to an upper limit for the majorana mass of $m_{\beta\beta} < (0.11 - 0.26)$ eV using the present ranges for Nuclear Matrix Elements. [1]

Improved PSD methods and a new LAr system for Phase II resulted in a Background Index (BI) for BEGes of $(0.6^{+0.3}_{-0.2}) \times 10^{-3} \frac{\text{cts}}{\text{keV kg yr}}$ [1]. This value will be referenced at the end of the thesis.

A complete spectrum with all cuts is given in figure 2.4.

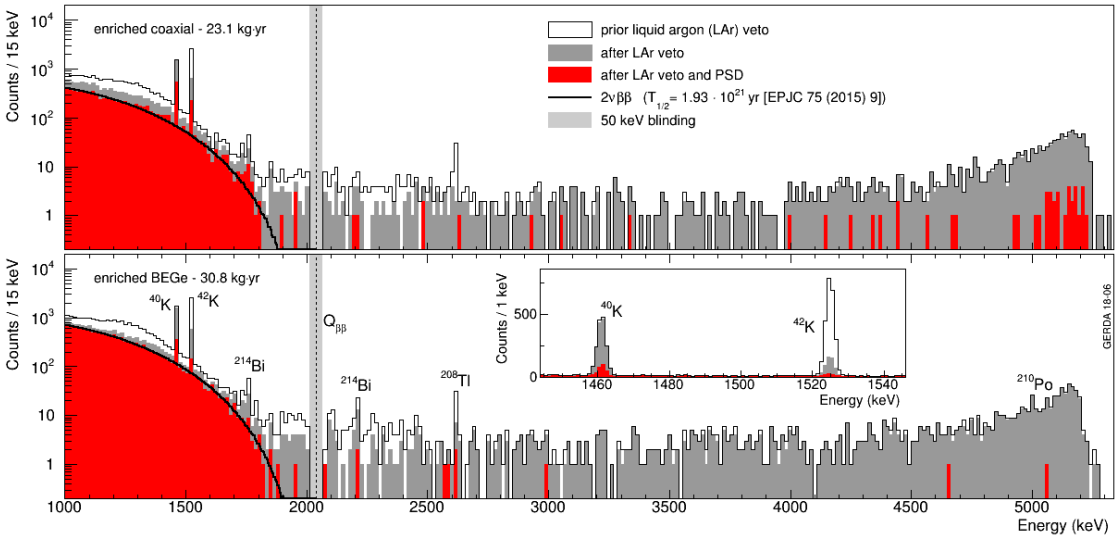

Figure 2.4.: Complete spectrum of the GERDA data with separate LAr and PSD cuts from [1]

3. Background in GERDA

3.1. General Background

Based on screening measurements the Phase II data was fitted with Probability Density Functions for various background sources leading to an extensive background model shown in figure 3.1. The ^{39}Ar β^- background in the region below 750 keV was cut out. The most obvious feature comes from the $2\nu\beta\beta$ decay of ^{76}Ge, which was calculated using a Monte-Carlo simulation assuming an homogeneous distribution of ^{76}Ge inside of each detector. It is the major contribution in the region from 600 keV to 1500 keV. The α background is mainly produced by ^{210}Po. It is expected to be located on the detector surface. [19]

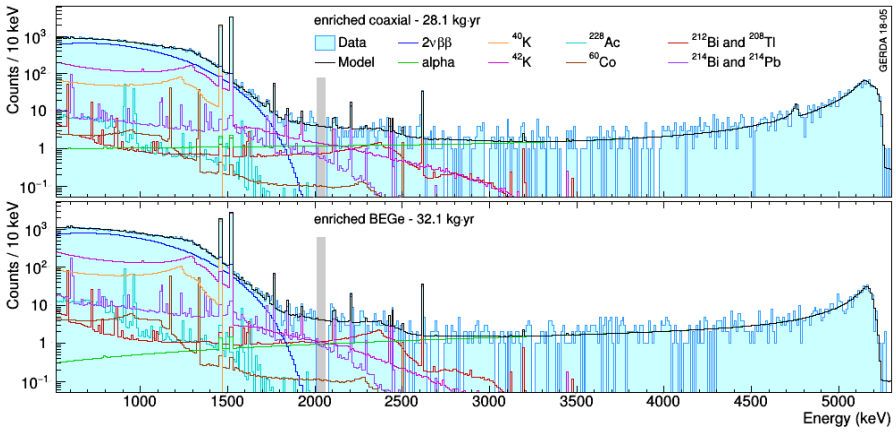

Figure 3.1.: Complete background model from [1]

^{40}K, as one of the significant sources of natural radioactivity, is expected in the assembly of the experiment. Synthetic ^{60}Co on the other hand can be found in the holders and the detectors itself. The main γ background comes from ^{212}Bi/^{208}Tl in the decay chain of ^{228}Th and ^{214}Bi/^{214}Pb in the ^{226}Ra chain. It originates from various sources within the setup and is compatible with screening results. ^{214}Bi and ^{214}Pb are the only β decaying isotopes which are able to emit γ-rays with energy inside the Region Of Interest (ROI). [19]

3.2. ^{42}K Background

Due to the natural occurrence induced by cosmogenic radiation, ^{42}Ar is homogeneously distributed inside LAr. ^{42}Ar decays into ^{42}K ions, which is a β^- emitter and has a endpoint energy of 3.5 MeV. ^{42}K has a half-life of 12.4 h, whereas ^{42}Ar has a half-life of 32.9 yr [23]. The long half-life is responsible for the background, even if it is stored in the cryostat in GERDA for a long time. The γ-line of ^{42}K at 1525 keV and the β contribution towards higher energies is clearly visible in the spectrum (cf. figure 3.1).

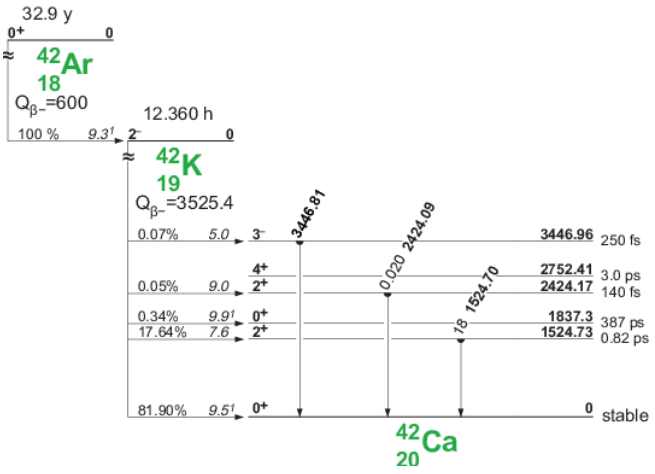

Figure 3.2.: Decay scheme of ^{42}Ar from [22]

Since the ^{42}K ions are charged, they are affected by the bias voltage of the detector and accumulate on the detector surface. The great LAr mass directly near the detectors produces the largest contribution to the background. Therefore it is constrained by the NMS.

A large fraction of the detector surface is n^+ doped and thus insensitive to radiation. Because of the high endpoint energy of ^{42}K, some β particles can permeate through this layer and deposit energy inside the active volume near the n^+ surface. Additionally, a transition layer between active and dead volume with no electric field is generated. Charges inside this layer slowly diffuse towards the active volume producing a slow pulse (cf. chapter 5.3).

These high energy electrons from accumulated ^{42}K near the detector surface are able to increase the background level in the ROI, which is centered around $Q_{\beta\beta} = 2039$ keV, significantly. [22]

4. Data Acquisition and Analysis

The data taking in GERDA is structured in runs. Run 52 from Phase I during Phase II commissioning will be used in the further investigation. Only two of the seven strings (4 and 6) in Run 52 were equipped with a Nylon Mini Shroud, as described by figure 4.1.

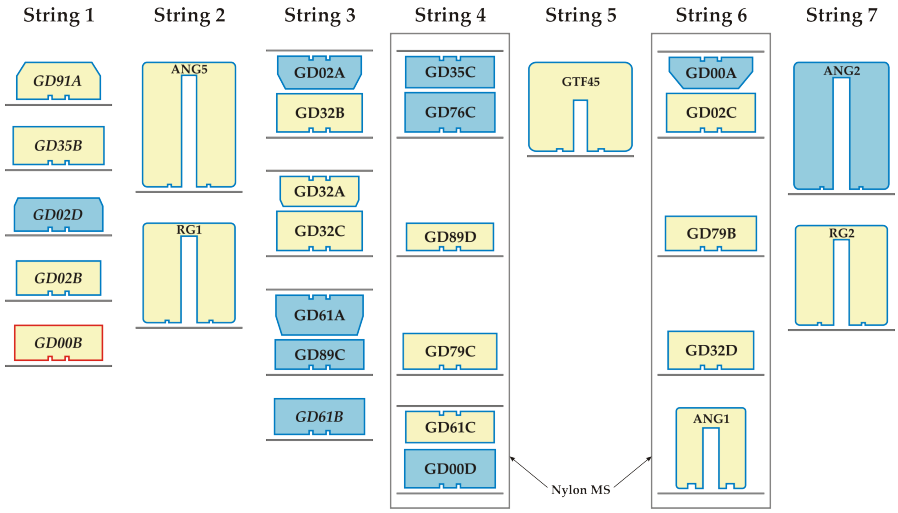

Figure 4.1.: String Configuration in Run 52 from [24]

Strings 1, 3, 4 and 6 contain only BEGe detectors (GDxxx). The enriched semi-coaxial detectors are located in string 2 and 7 (RGx and ANGx), whereas string 5 contains a detector with natural Ge (GTF45). The GD00B detector is off in this configuration. Blue detectors are equipped with a passivation layer inside the groove between p^+ and n^+ surface. The yellow ones have this layer removed.

4.1. Detector Stability

Weekly energy calibration with ^{228}Th is one of the steps in a successful data taking in GERDA to secure a properly defined energy scale. In Run 52, calibrations were made on the following dates: 16.11.2015, 20.11.2015, 23.11.2015, 01.12.2015 and 07.12.2015.[24]

The typical 2615 keV line from ^{208}Tl is used to determine a potential drift in the detectors gain. Furthermore, Test Pulses (TPs) are injected each 20 s into the read-out electronics. Only data during a stable operation is used in the following analysis. Figure 4.2 shows two of these TP distributions, one stable, the other one only used for Anti Coincidence, because of major instabilities in ANG2. [25]

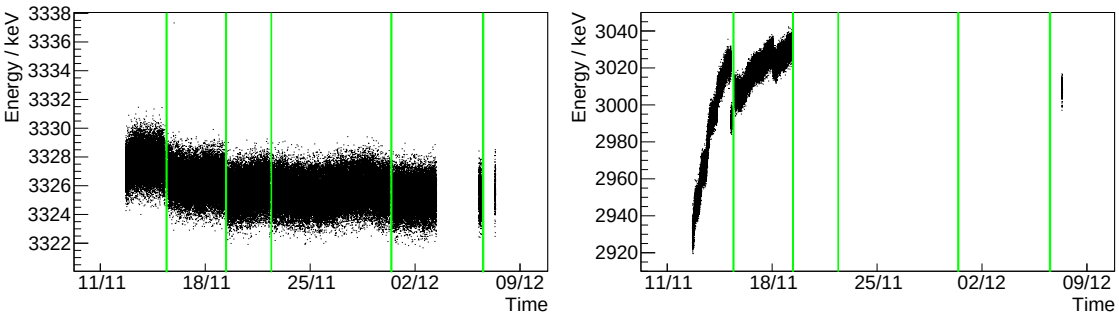

(a) GD91A detector

(b) ANG2 detector

Figure 4.2.: Energy distribution of test pulses. The green lines indicate the calibration times

Data Selection

Unfortunately, four detectors (GD32C, GD61A, GD89D, GD79C) were found to have an unstable Amplitude over Energy (A/E) value in the calibration. A/E values are used in chapter 5.3 for PSD. This instability arises from changing noise level in the electronics. An example of this discontinuity after one of the calibrations can be found in figure 4.3. The effect is also visible in the calibration data in the appendix (cf. figure A.0) as a shifted Single Site Event (SSE) band. Therefore, an individual data selection was made in which data after the last measurement in the fourth calibration was cut out. Less active time results in a lower exposure for the four detectors in the upcoming calculations.

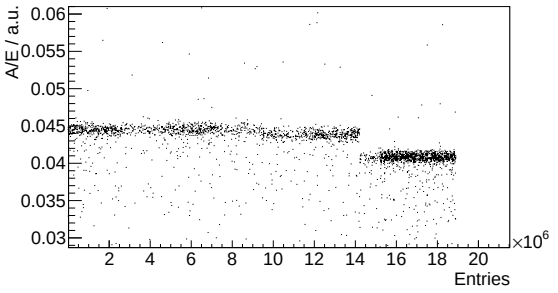

Figure 4.3.: A/E discontinuity of GD61A

The lower exposure has to be considered also in the calculations before PSD for a comparison afterward.

4.2. Detector Exposure

For normalization of the BI and the spectra, a calculation of the detector exposure for each BEGe detector is done.

The summed exposure for string 1 and 3 is $\epsilon_{\overline{NMS}} = 0.42\,\mathrm{kg\,yr}$, whereas the exposure for strings 4 and 6 with NMS is $\epsilon_{NMS} = 0.36\,\mathrm{kg\,yr}$. Both are assumed to have no significant uncertainty, because the uncertainty of the detector masses is less than 0.22 % assuming 1 g deviation.

4.3. Background Index

The BI provides information on the background level around $Q_{\beta\beta}$. It is assumed to be flat which is confirmed by the background model.

According to [24] the energy window for BI calculation spans from 1930 keV to 2190 keV, above the 1922 keV γ line from ^{42}K and below the γ line of ^{214}Bi at 2204 keV. Three regions at $Q_{\beta\beta} \pm 5$ keV, (2104 ± 5) keV and (2119 ± 5) keV from lines of ^{208}Tl and ^{214}Bi, respectively, are excluded. Thus the window contains a total of 230 keV.

Using the BI as a quantitative measure for background reduction, the effect of a NMS, the background suppression by PSD and LAr vetoing are presented in the following chapters.

The BI of GERDA is typically given in $10^{-3}\ \frac{\text{cts}}{\text{keV yr}}$, because the goal for Phase II was of this order.

5. Background suppression

The major strength of GERDA is low background, which is achieved by passive and active background suppression. Passive suppression describes shielding by e.g. a NMS, active rejection uses offline analyses like PSD and the LAr veto.

5.1. Nylon Mini Shroud

In Phase I a copper cylinder, known as Mini Shroud (MS), was placed around the detector array to prevent ^{42}K decays near the detector surface. This mechanical barrier inhibits a drifting of this isotope towards the array by blocking the electric fields and thus reducing the overall background as ^{42}K accumulation can only happen inside the volume defined by the MS.

With the LAr veto in Phase II the MS could no longer be used since scintillation light coming from inside the MS volume would not have been detected by the LAr veto. Alternatively, a high-purity NMS was developed which does not shield electric fields but serves as a simple barrier. The NMS is coated with TPB on both sides allowing the shifting of the scintillation light and the transport of light through the nylon. The quantitative effect of this shroud is presented.

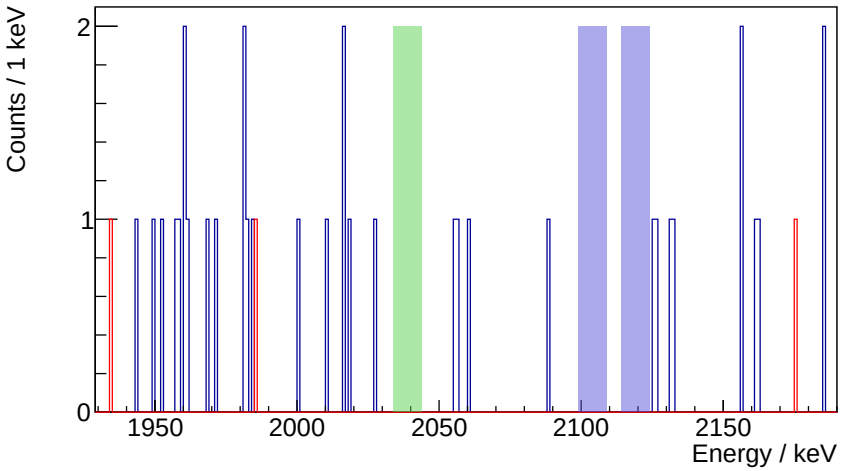

Figure 5.1.: Effect of the NMS. The blue histogram displays data without NMS, the red with. The green region is centered around $Q_{\beta\beta}$ and the two blue regions mark the typical lines described in chapter 4.3.

Figure 5.1 is showing the summed counts of strings 1,3 and strings 4,6 inside the BI

window. With no NMS, 34 events are recorded. When using a shroud, the count rate goes down to three. Using the above calculated exposure and the total width of the BI window, a normalized BI is figured for both cases:

$$BI_{\overline{NMS}} = (355.5^{+66.2}_{-59.3}) \times 10^{-3} \, \frac{\text{cts}}{\text{keV kg yr}} \tag{5.1}$$

$$BI_{NMS} = (35.8^{+27.5}_{-22.6}) \times 10^{-3} \, \frac{\text{cts}}{\text{keV kg yr}} \tag{5.2}$$

The uncertainties are determined under the assumption of a background free measurement using the approach of [26], suitable for this Poissonian process. The confidence level is 68.27 % (1σ).

Furthermore, a BI for the semi coaxial detectors (ANGx and RGx) can be obtained.

$$BI_{coax} = (107.5^{+37.3}_{-31.1}) \times 10^{-3} \, \frac{\text{cts}}{\text{keV kg yr}} \tag{5.3}$$

The BI_{coax} is lower than the BI for BEGe detectors. This is due to their lower surface to volume fraction. With lower surface area, less ^{42}K decays happen with regard to the detector mass. Another aspect is the thicker dead layer of coaxial detectors.

To conclude, the deployment of the NMS can suppress the background by one order of magnitude down to $10^{-2} \, \frac{\text{cts}}{\text{keV kg yr}}$. This is a clear indication that the by far biggest fraction of the background, in the dataset without a NMS, is coming from ^{42}K, because the NMS is able to suppress it.

To show the effect of different suppression methods, string 1 and 3 are considered hereafter, since they provide a strong ^{42}K background.

5.2. Liquid Argon Veto

The hardware and technique of the LAr veto is described in 2.1.2. If an event deposits a certain amount of energy in LAr, a distinct amount of light, e.g. bremsstrahlung of β particles is produced. The PMTs and SiPMs produce a signal, which is aligned to the corresponding signal from the germanium detectors. If the veto signal is above threshold inside a time frame in the order of 5 µs, the event is vetoed. This takes the characteristic timing of the LAr scintillation process into account.

Liquid Argon Veto Cut

The LAr cut is already implemented in top level data. A simple flag with a boolean value is used to discard events which coincide with light detection. Like before, figure 5.2 displays events inside the background window. A 20.6 % survival fraction can be obtained by the LAr when 34 events are reduced to 7. Finally, a BI can be calculated once again.

$$BI_{LAr} = (73.2^{+34.6}_{-28.7}) \times 10^{-3} \, \frac{\text{cts}}{\text{keV kg yr}} \tag{5.4}$$

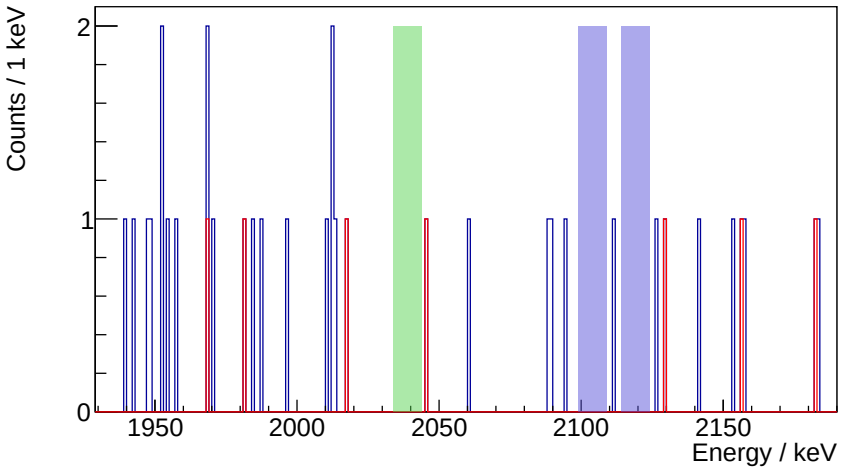

Figure 5.2.: LAr veto cut. Seven events survive the vetoing

A comparison of this results with expectations from Monte Carlo simulations is possible. A suppression factor of 2.63 ± 0.10 for homogeneously distributed ^{42}K in LAr is provided in [27]. This corresponds to a survival fraction of $(38.0 \pm 1.4)\,\%$.

Liquid Argon Acceptance

Natural radioactivity in the LAr, which is mainly coming from ^{39}Ar, is able to produce light. According to [28], the natural activity for ^{39}Ar is $1.01^{\pm 0.02(\text{stat})}_{\pm 0.08(\text{sys})}\ \frac{\text{Bq}}{\text{kg}}$. Furthermore, a dark rate of the LAr read-out channels is present. Due to the statistical nature of these processes, a small amount of events in the germanium detectors is happening in random coincidence with light deposition and is categorized as a decay inside e.g. the LAr and not registered. To examine this acceptance for false vetoed events, TPs can be used.

TPs are in that context true events, because they do not produce any light. A simple division of the number of all events from TPs and events, where no LAr veto flag fired, yields an acceptance of $(98.0 \pm 0.7)\,\%$.

5.3. Pulse Shape Discrimination

PSD is an active background suppression method. The PSD in this analysis is referring to the procedure for BEGe detectors from Phase II: A monoenergetic cut based on the ratio of the current pulse over the deposited energy A/E [18].

$0\nu\beta\beta$ events deposit energy very localized (SSE) in the detector, an event with multiple energy depositions (Multi Site Event (MSE)) is likely to be a γ.

Three main interactions of γ-rays in matter are possible:

- **Photoelectric effect**
  At low energies up to around 100 keV, the incident γ can transfer its full energy to an electron, which is then ejected.
- **Compton scattering**
  Higher energy of the γ results in multiple scattering on the electrons and piecemeal deposition of energy. This process is favored at around a few MeV.
- **Pair production**
  Above the energy of 1022 keV, a conversion of the γ into an electron positron pair is possible.

Double Escape Peak

A Double Escape Peak (DEP) occurs whenever a γ produces an electron positron pair and both of the two 511 keV photons from the annihilation of the positron escape the detection. If only one photon is detected, a Single Escape Peak (SEP) appears. The electron is stopped in the detector. Because the energy deposition is very localized, DEPs can be used as a proxy for $0\nu\beta\beta$ events.

As already mentioned in 4.1, ^{228}Th is used for calibration. It is dominated by the γ-rays from ^{208}Tl. The 2615 keV line (Full Energy Peak (FEP)) of ^{208}Tl is marked in figure 5.3. Hence, the SEP is located 511 keV next to the FEP at 2104 keV. The DEP peak can be found at 1593 keV as a high density region in the SSE band and is not to be mixed up with the FEP of ^{208}Tl at 1621 keV. [29]

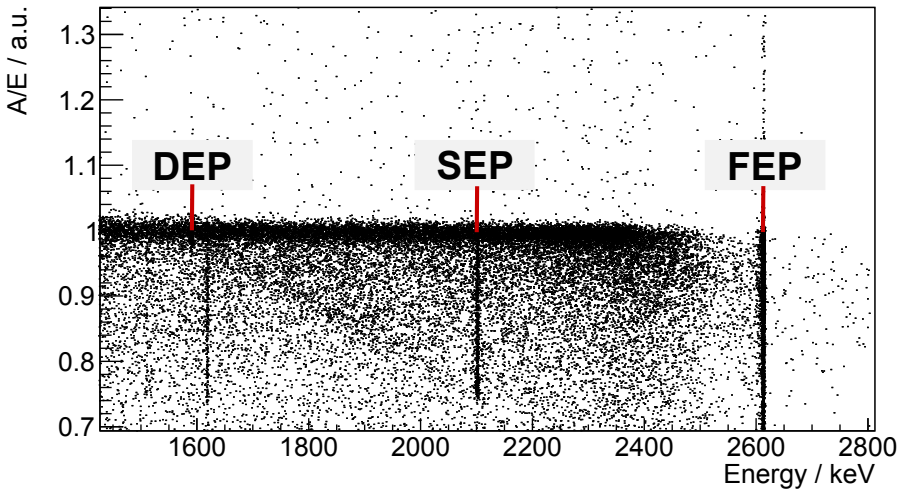

Figure 5.3.: Normalized calibration spectrum of GD32D for the first calibration in Run 52

PSD for BEGes

Figure 5.4 is showing a comparison between a SSE and a MSE. The amplitude of the red pulses determines the E value. Differentiating this charge pulse leads to the blue current pulses, which maximum amplitude is A. The SSE event has a high amplitude of the current pulse (A) and creates a single peak. MSE events on the other hand are split off in multiple peaks, due to similar drift times for all interactions. The BEGe detectors feature an impurity gradient in one axis, hence charges move to the middle of the detector where they are drifted towards the p^+ electrode by the applied high voltage [18]. A one-parameter cut arises from the fact, that similar events own a similar A/E value, no matter where the deposition happens. Thus, the MSE pulses have a much smaller amplitude and therefore a lower A/E value.

Furthermore, p^+ and n^+ surface events can also be distinguished by their pulse shape. The p^+ events feature a much higher A than the SSE events. Events on n^+ surface are characterized by a long rise time. The accumulation of ^{42}K discussed in 3.2 happens on the detector surface. High energy electrons are able to penetrate inside the active volume. The bigger fraction generates charges inside the dead layer, which are able to diffuse into the n^+ surface. This leads to a slow rising edge of the charge pulse, a so-called slow pulse. Thus, most of ^{42}K decays produce such slow pulses and can, therefore, be removed by a strong cut on low A/E values. A strong noise dependence of this cut can be observed since noise increases the width of the SSE band. Strong ^{42}K suppression is hence only possible under good noise conditions.

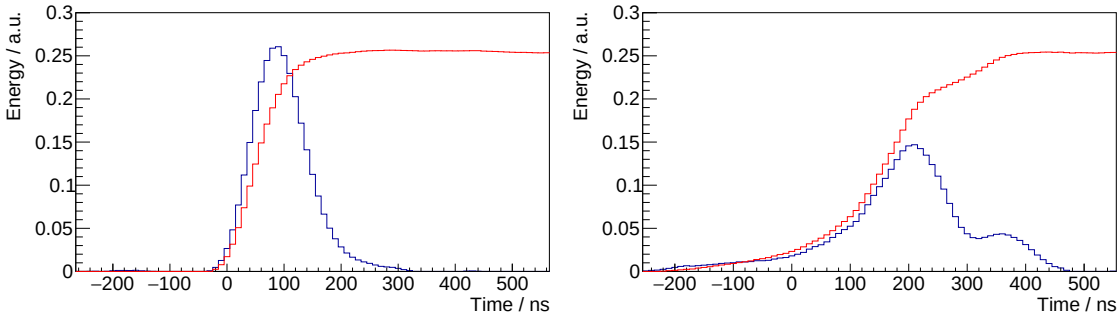

(a) SSE Event

(b) MSE Event

Figure 5.4.: Single pulse shapes

A/E Calibration

Since data during the commissioning of Phase II is used, the calibration for the A/E cut is done similarly to Phase II. The steps and methods are adapted from [18]. The A/E values are calibrated in such way that the SSE band is centered around $A/E = 1$ and normalized to the mean A/E value in the DEP. As the A/E values have a small energy dependence, it is assumed that the SSE band behaves linear from 0.5 MeV to 3 MeV.

Possible sources for this are increased noise at lower energies or the increased emission of bremsstrahlung at higher energies. It is important to only include specific energy slices with a Compton background where no transition lines are present. The slices are chosen according to the appendix of [18]. The broadening of the band towards lower energies, which is due to noise, is neglected in this work and affects mainly lower energies. [18]

After fitting the linear energy of the SSE band to get a mean A/E value, the DEP is examined. It has a Gaussian shape and a constant Compton background is present, which is subtracted statistically using the sidebands of the peak. All detectors have a slightly different A/E characteristic and require a different calibration.

The low cut is done at 90 % acceptance concerning the DEP, whereas the high cut is set at 4σ of the DEP A/E resolution. The parameter for the resulting low and high cuts including the Full width at half maximum (FWHM) of the Gaussian fit for the DEP included in table A.2. The low cut values reach from 0.978 to 0.991 and the high cut values from 1.029 to 1.068. The FWHM can be calculated with the standard deviation $\mathrm{FWHM} = 2\sqrt{2\ln 2}\sigma$. The high cut is able to remove p^+ events from the data, whereas the low cut rejects MSE and n^+ events. An example of this cut is given in figure 5.5. All events are cut out by the A/E cut for this detector.

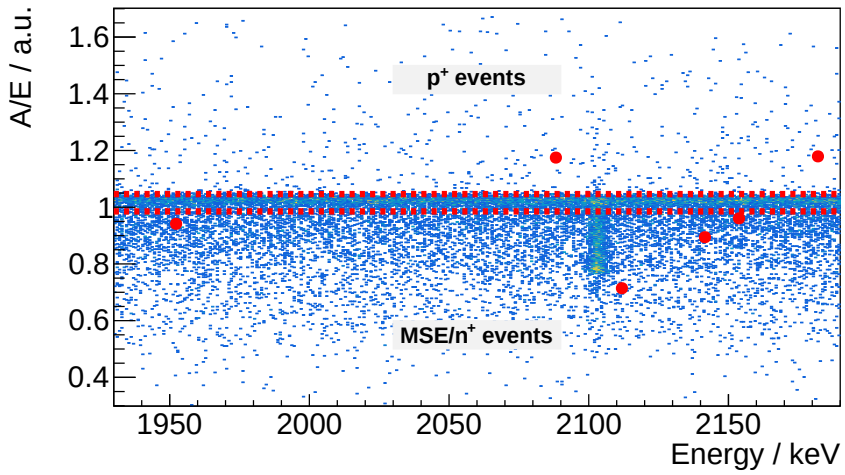

Figure 5.5.: GD00B PSD cut (events are marked in red)

A/E Cut

After the calibration for every BEGe detector, the described cut is applied. All used detectors with their calibration and physic data can be found in the appendix.

The cut is able to reduce the amount of accepted events in the BI window from 34 down to 6 (cf. figure 5.6).

$$BI_{PSD} = (62.7^{+34.3}_{-22.7}) \times 10^{-3} \, \frac{\mathrm{cts}}{\mathrm{keV\,kg\,yr}} \tag{5.5}$$

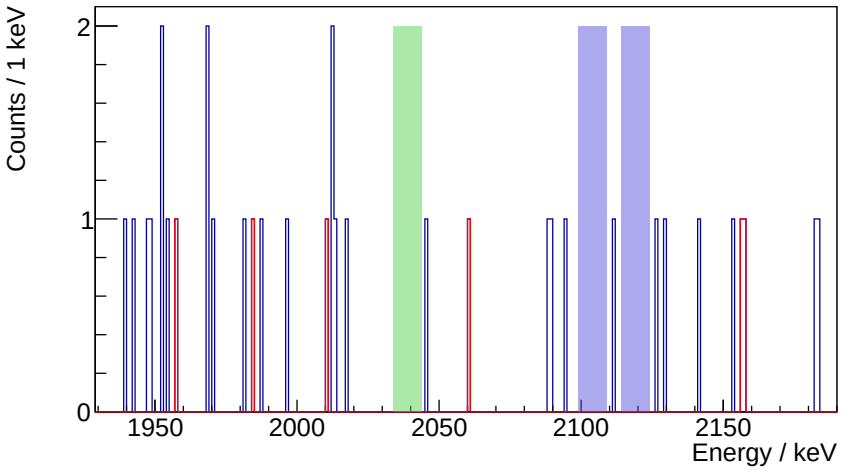

Figure 5.6.: Effect of the PSD cut. The blue histogram displays data before the cut, the red after. Six events remain after the cut.

Combining LAr veto and PSD

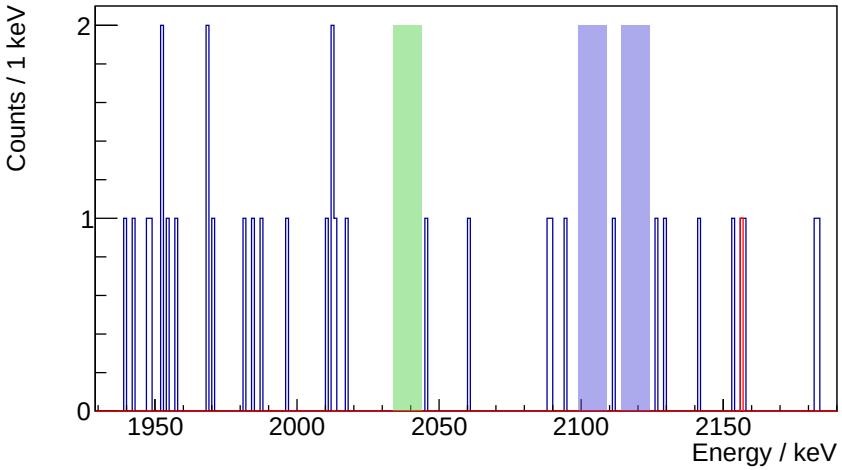

Figure 5.7.: Combined LAr veto and PSD cut. Only one event remains after the cut.

The two presented suppression methods are combined in the actual analysis. Only events with a A/E ratio in the acceptance limit and below the threshold for LAr veto are kept. The corresponding BI for one count inside the BI window is

$$BI_{LAr+PSD} = (10.4^{+18.3}_{-6.6}) \times 10^{-3} \, \frac{\text{cts}}{\text{keV kg yr}}. \tag{5.6}$$

Interplay between the two suppression methods works flawlessly, since different types of events get rejected by each method. This results in a far lower survival fraction than two independent cuts would provide (cf. chapter 6).

6. Results/Comparison

Table 6.1.: Summary of results and comparison with GERDA data from [1] and [24]

BEGe Dataset	without NMS	with NMS	GERDA Phase II
Exposure / kg yr	0.416	0.364	30.8
BI total / cts keV^{-1} kg^{-1} yr^{-1}	$355.5^{+66.2}_{-59.3}$	$35.8^{+27.5}_{-22.6}$	$14.1^{+1.5}_{-1.4}$
... after LAr cut	$73.2^{+34.6}_{-28.7}$	$23.9^{+26.9}_{-15.0}$	$5.9^{+1.0}_{-0.9}$
... after PSD cut	$62.7^{+34.3}_{-22.7}$		$3.2^{+0.7}_{-0.6}$
... after LAr+PSD cut	$\mathbf{10.4^{+18.3}_{-6.6}}$		$0.6^{+0.3}_{-0.2}$

The results of the background suppression analysis are presented in table 6.1. When using the LAr veto system, 20.6 % of the events in the dataset without a NMS survived the cut. PSD was able to further decrease this to 17.6 %. If both cuts are applied, only a single event remained which corresponds to a survival probability of 2.9 %.

The GERDA Phase II dataset was using a NMS and can be compared to the corresponding dataset. The calculated BI values match the GERDA results inside the uncertainties, although the presented expectation values are two to four times higher.

Assuming, that the NMS is able to suppress ^{42}K events, at least the BI difference of $319.7^{+93.7}_{-81.9}$ $\frac{\text{cts}}{\text{keV kg yr}}$ is induced by ^{42}K decays and contributes to the background. A comparison with the BIs after the different cuts allows the determination of upper limits for ^{42}K suppression efficiency by them. In the worst case, all remaining events after the cut are still ^{42}K events.

Therefore, the expectation values for the upper limits are 22.9 %, 19.6 % and 3.3 % for LAr veto, PSD and the combined cut, respectively. Systematic uncertainties of the upper limits are neglectable. Calculating the statistic uncertainties would involve complex Poissonian error propagation which is beyond the scope of this thesis.

In this dataset, combined LAr and PSD cuts are able to suppress the central ^{42}K survival fraction down to $\approx 3.3\,\%$.

7. Conclusion/Outlook

The understanding of the background in GERDA is essential. Evaluating suppression methods is an important step in this process, as they can be compared and improved.

The ^{42}K background in GERDA can be further restrained in various ways. On the one hand, stronger passive shielding via a smaller NMS is possible. The size is limited by the detectors and holders themselves. Also, the dead layer thickness can be reduced to prevent charge deposition inside. On the other hand, active suppression can be evaluated. Lowering the noise in the read-out electronics leads to a thinner SSE band and therefore a stronger A/E cut. This could e.g. be done with a first front end amplifier stage near the detector decreasing the noise sensitive cable length.
According to [30], underground argon with a significantly lower ^{39}Ar and ^{42}K concentration can be used to decrease the amount of ^{42}K. Also, a better light yield would be present in underground argon.

Since light transport through the NMS is not lossless, a read-out fiber within the array would improve this.

Moreover, spiked ^{42}Ar was used in [22] for better tests of the suppression methods.

A recent run after the modification on the Phase II setup used partial covering with NMSs on some detectors again. This data could be used to perform a similar analysis with better statistics. A further investigation at the TUM test cryostat is planned [24].

Data taking in the background-free regime is necessary to reach for higher sensitivities. The recently formed LEGEND Collaboration will continue the search for $0\nu\beta\beta$ decays in ^{76}Ge with follow up experiments in two stages. The first stage will use up to 200 kg detector material and is therefore called LEGEND-200. It will be deployed in the existing infrastructure at LNGS. In the next phase, a 1000 kg experiment is planned. Especially for this purposes, ^{42}K suppression will be of major interest. [31]

A. Appendix

A.1. Exposure

Table A.1.: Exposure of all detectors (ANG2 excluded). Each string is grouped.

Name	Mass / kg	Exposure / kg yr
GD91A	0.627	0.035
GD35B	0.810	0.045
GD02D	0.662	0.037
GD02B	0.625	0.035
GD00B	0.697	0.039
ANG5	2.746	0.153
RG1	2.110	0.118
GD02A	0.545	0.030
GD32B	0.716	0.040
GD32A	0.458	0.026
GD32C	0.743	0.041
GD61A	0.731	0.041
GD89C	0.595	0.033
GD61B	0.751	0.042
GD35C	0.634	0.035
GD76C	0.824	0.046
GD89D	0.526	0.029
GD79C	0.812	0.045
GD61C	0.634	0.035
GD00D	0.813	0.045
GTF45_2	2.312	0.129
GD00A	0.496	0.028
GD02C	0.788	0.044
GD79B	0.736	0.041
GD32D	0.720	0.040
ANG1	0.958	0.053
RG2	2.166	0.121

A.2. A/E Calibration

Table A.2.: Normalized A/E cut calues in σ, and FWHM of the DEP for all BEGe detectors. Only string 1+3 are used in the analysis. Each string is grouped.

Name	Low cut	High cut	FWHM DEP
GD91A	0.987	1.041	0.024
GD35B	0.987	1.041	0.024
GD02D	0.980	1.063	0.037
GD02B	0.984	1.049	0.029
GD00B	0.985	1.046	0.027
GD02A	0.989	1.034	0.020
GD32B	0.988	1.039	0.023
GD32A	0.987	1.041	0.024
GD32C	0.985	1.046	0.027
GD61A	0.983	1.053	0.031
GD89C	0.985	1.048	0.028
GD61B	0.986	1.042	0.025
GD35C	0.991	1.029	0.017
GD76C	0.989	1.033	0.019
GD89D	0.990	1.032	0.019
GD79C	0.988	1.037	0.022
GD61C	0.978	1.068	0.024
GD00D	0.988	1.039	0.023
GD00A	0.989	1.035	0.021
GD02C	0.989	1.035	0.020
GD79B	0.989	1.035	0.021
GD32D	0.988	1.036	0.021

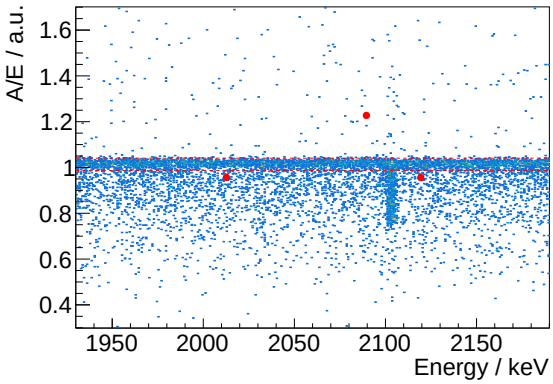

(a) GD91A

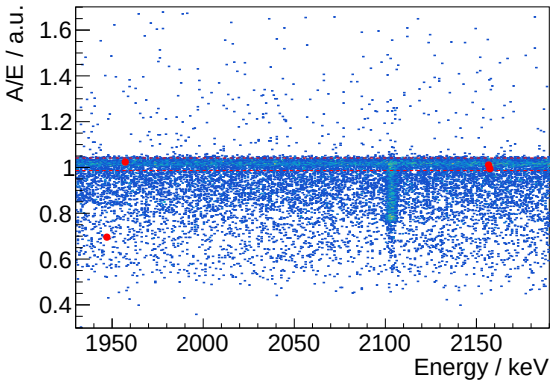

(b) GD35B

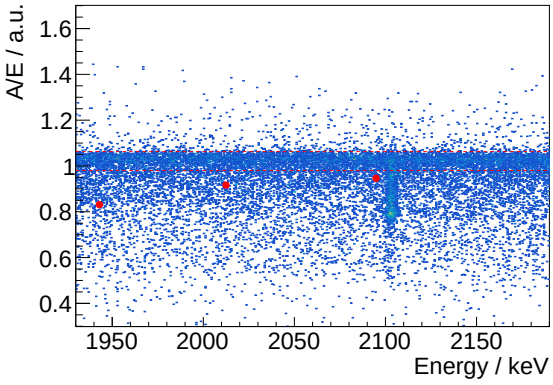

(c) GD02D

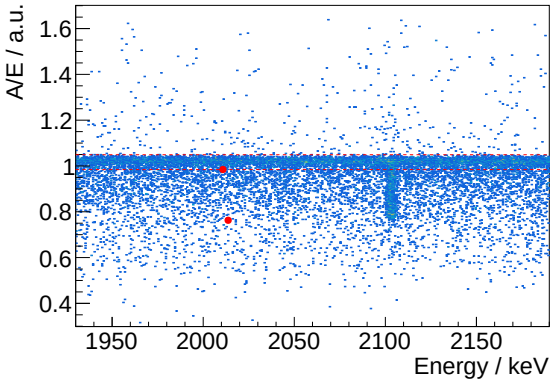

(d) GD02B

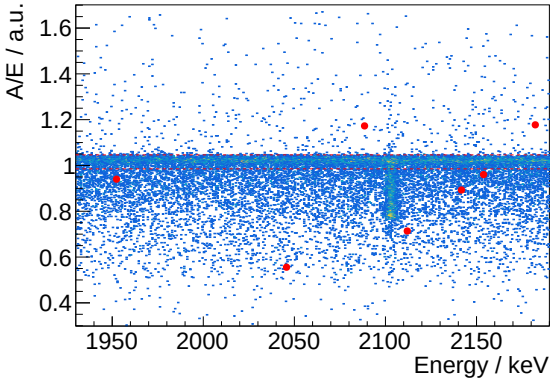

(e) GD00B

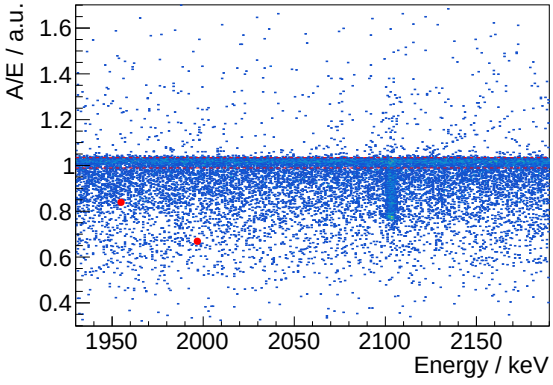

(f) GD02A

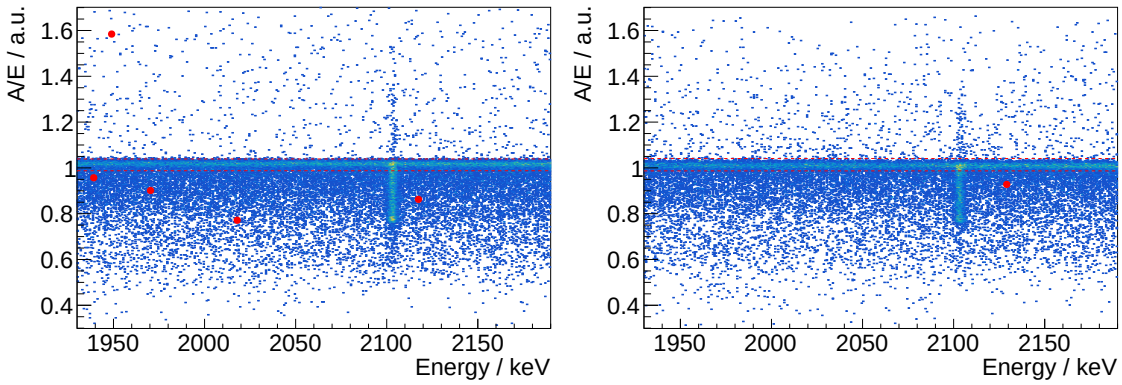

(g) GD32B

(h) GD32A

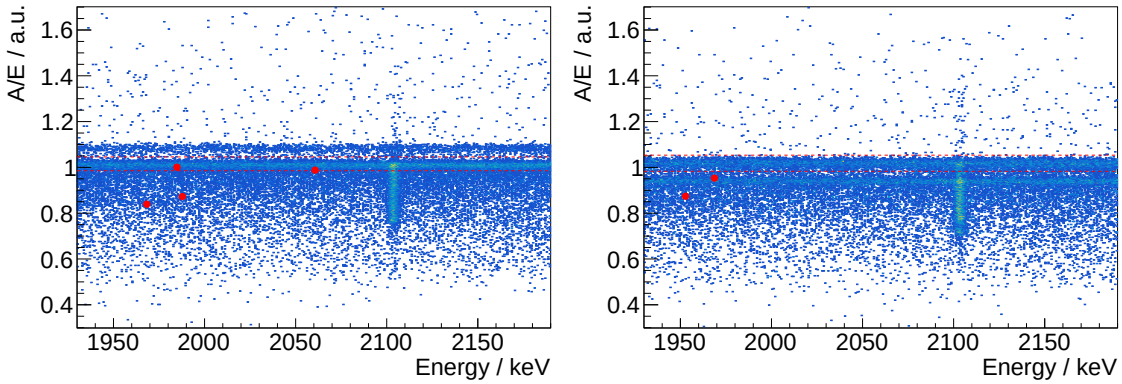

(i) GD32C before data selection

(j) GD61A before data selection

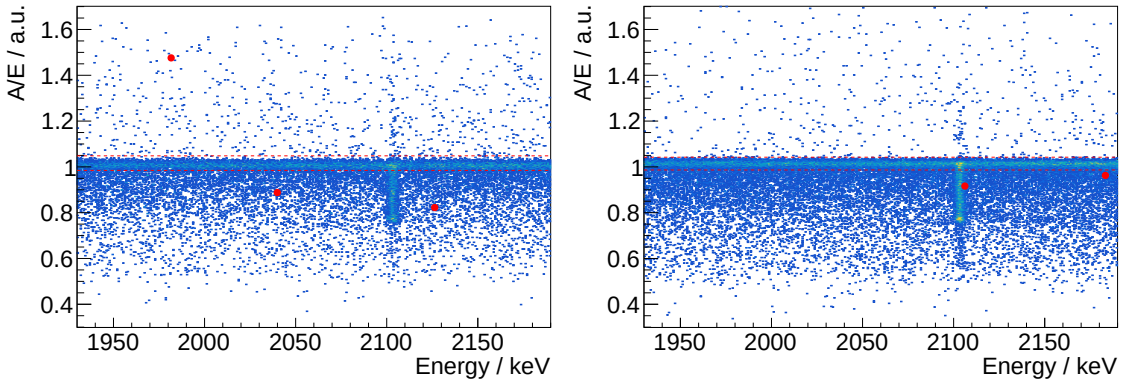

(k) GD89C

(l) GD61B

Figure A.0.: A/E Cuts inside the BI window for used detectors (string 1+3). Events are marked with a red dot. The acceptance lines represent the normalized lower and upper cut. The shifted SSE band in detector 10 and 11 are cut for analysis.

Bibliography

[1] Anna Julia Zsigmond. *New results from GERDA Phase II*. 2018. DOI: 10.5281/zenodo.1287604. URL: https://doi.org/10.5281/zenodo.1287604.

[2] Wolfgang Pauli. "Zur älteren und neueren Geschichte des Neutrinos". In: *Physik und Erkenntnistheorie*. Springer, 1984, pp. 156–180.

[3] Frederick Reines et al. "Detection of the free antineutrino". In: *Physical Review* 117.1 (1960), p. 159.

[4] G Danby et al. "Observation of High-Energy Neutrino Reactions and the Existence of Two Kinds of Neutrinos". In: *Phys. Rev. Lett.* 9.1 (July 1962), pp. 36–44. DOI: 10.1103/PhysRevLett.9.36. URL: https://link.aps.org/doi/10.1103/PhysRevLett.9.36.

[5] DONUT Collaboration. "Observation of Tau Neutrino Interactions". In: (Dec. 2000). DOI: 10.1016/S0370-2693(01)00307-0. arXiv: 0012035 [hep-ex]. URL: http://arxiv.org/abs/hep-ex/0012035%20http://dx.doi.org/10.1016/S0370-2693(01)00307-0.

[6] K. Zuber. *Neutrino Physics*. 2nd ed. CRC Press, 2012.

[7] Bruno Pontecorvo. "Neutrino Experiments and the Problem of Conservation of Leptonic Charge". In: *JETP* 53.5 (1968). URL: http://www.jetp.ac.ru/cgi-bin/dn/e%7B%5C_%7D026%7B%5C_%7D05%7B%5C_%7D0984.pdf.

[8] Ziro Maki, Masami Nakagawa, and Shoichi Sakata. "Remarks on the unified model of elementary particles". In: *Prog. Theor. Phys.* 28 (1962), pp. 870–880. DOI: 10.1143/PTP.28.870.

[9] Bogdan Povh et al. *Teilchen und Kerne*. 9th ed. Springer Spektrum, 2014.

[10] SNO Collaboration. "Direct Evidence for Neutrino Flavor Transformation from Neutral-Current Interactions in the Sudbury Neutrino Observatory". In: (Apr. 2002). DOI: 10.1103/PhysRevLett.89.011301. arXiv: 0204008 [nucl-ex]. URL: http://arxiv.org/abs/nucl-ex/0204008%20http://dx.doi.org/10.1103/PhysRevLett.89.011301.

[11] The Super-Kamiokande Collaboration and Y. Fukuda et Al. "Evidence for oscillation of atmospheric neutrinos". In: (July 1998). DOI: 10.1103/physrevlett.81.1562. arXiv: 9807003 [hep-ex]. URL: http://arxiv.org/abs/hep-ex/9807003%20http://dx.doi.org/10.1103/PhysRevLett.81.1562.

[12] Nobelprice.org. *The Nobel Prize in Physics 2015*. 2015. URL: https://www.nobelprize.org/nobel%7B%5C_%7Dprizes/physics/laureates/2015/ (visited on 07/02/2018).

[13] C. F v Weizsäcker. "Zur Theorie der Kernmassen". In: *Zeitschrift für Physik* (1935). ISSN: 14346001. DOI: 10.1007/BF01337700.

[14] Brianna J Mount, Matthew Redshaw, and Edmund G Myers. "Double-beta-decay Q values of Se-74 and Ge-76". In: *Phys. Rev.* C81 (2010), p. 32501. DOI: 10.1103/PhysRevC.81.032501.

[15] Ethan Siegel. *Could dark energy be caused by frozen neutrinos?* URL: https://medium.com/starts-with-a-bang/could-dark-energy-be-caused-by-frozen-neutrinos-ac243a7e9f7d.

[16] Michael Duerr, Manfred Lindner, and Kai Zuber. "Consistency test of neutrinoless double beta decay with one isotope". In: *Physical Review D - Particles, Fields, Gravitation and Cosmology* 84.9 (Mar. 2011). ISSN: 15507998. DOI: 10.1103/PhysRevD.84.093004. arXiv: arXiv:1103.4735v1. URL: http://arxiv.org/abs/1103.4735%20http://dx.doi.org/10.1103/PhysRevD.84.093004.

[17] M. Agostini et al. "Upgrade for Phase II of the GERDA Experiment". In: (Nov. 2017). DOI: 10.1140/epjc/s10052-018-5812-2. arXiv: 1711.01452. URL: http://arxiv.org/abs/1711.01452%20http://dx.doi.org/10.1140/epjc/s10052-018-5812-2.

[18] Victoria Elisabeth Wagner. "Pulse Shape Analysis for the GERDA Experiment to Set a New Limit on the Half-life of $0\nu\beta\beta$ Decay of Ge-76". PhD thesis. 2017.

[19] The GERDA Collaboration, M Agostini, et al. "The background in the neutrinoless double beta decay experiment GERDA". In: *ArXiv e-prints* (June 2013). arXiv: 1306.5084 [physics.ins-det].

[20] M. Agostini et al. "Results on neutrinoless double beta decay of Ge-76 from GERDA Phase I". In: (July 2013). DOI: 10.1103/PhysRevLett.111.122503. arXiv: 1307.4720. URL: http://arxiv.org/abs/1307.4720%20http://dx.doi.org/10.1103/PhysRevLett.111.122503.

[21] M. Agostini et al. "Results on $\beta\beta$ decay with emission of two neutrinos or Majorons in Ge-76 from GERDA Phase I". In: (Jan. 2015). DOI: 10.1140/epjc/s10052-015-3627-y. arXiv: 1501.02345. URL: http://arxiv.org/abs/1501.02345%20http://dx.doi.org/10.1140/epjc/s10052-015-3627-y.

[22] A. Lubashevskiy et al. "Mitigation of Ar-42/K-42 background for the GERDA Phase II experiment". In: (Aug. 2017). DOI: 10.1140/epjc/s10052-017-5499-9. arXiv: 1708.00226. URL: http://arxiv.org/abs/1708.00226%20http://dx.doi.org/10.1140/epjc/s10052-017-5499-9%20http://arxiv.org/abs/1708.00226%7B%5C%%7D0Ahttp://dx.doi.org/10.1140/epjc/s10052-017-5499-9.

[23] Jun Chen and Balraj Singh. "Nuclear Data Sheets for A = 42". In: *Nuclear Data Sheets* 135 (July 2016), pp. 1–192. ISSN: 0090-3752. DOI: 10.1016/J.NDS.2016.06.001. URL: https://www.sciencedirect.com/science/article/pii/S0090375216300126.

[24] *Private Communication inside the GERDA Collaboration*. 2018.

[25] C. Bauer et al. "Background-free search for neutrinoless double-β decay of Ge-76 with GERDA". In: *Nature* 544.7648 (Mar. 2017), pp. 47–52. ISSN: 14764687. DOI: 10.1038/nature21717. arXiv: 1703.00570. URL: http://arxiv.org/abs/1703.00570.

[26] Gary J. Feldman and Robert D. Cousins. "A Unified Approach to the Classical Statistical Analysis of Small Signals". In: (Nov. 1997). DOI: 10.1103/PhysRevD.57.3873. arXiv: 9711021 [physics]. URL: http://arxiv.org/abs/physics/9711021%20http://dx.doi.org/10.1103/PhysRevD.57.3873.

[27] Björn Lehnert. "Search for $2\nu\beta\beta$ Excited State Transitions and HPGe Characterization for Surface Events in GERDA Phase II". PhD thesis. Technischen Universität Dresden, 2015.

[28] P. Benetti et al. "Measurement of the specific activity of Ar-39 in natural argon". In: (Mar. 2006). DOI: 10.1016/j.nima.2007.01.106. arXiv: 0603131 [astro-ph]. URL: http://arxiv.org/abs/astro-ph/0603131%20http://dx.doi.org/10.1016/j.nima.2007.01.106.

[29] M. Agostini et al. "Pulse shape discrimination for GERDA Phase I data". In: *European Physical Journal C* 73.10 (2013). ISSN: 14346052. DOI: 10.1140/epjc/s10052-013-2583-7. arXiv: 1307.2610.

[30] C. Galbiati and R. Purtschert. "Discovery of underground argon with low level of radioactive 39Ar and possible applications to WIMP dark matter detectors". In: (Dec. 2007). DOI: 10.1088/1742-6596/120/4/042015. arXiv: 0712.0381. URL: http://arxiv.org/abs/0712.0381.

[31] LEGEND Collaboration et al. "The Large Enriched Germanium Experiment for Neutrinoless Double Beta Decay (LEGEND)". In: (Sept. 2017). DOI: 10.1063/1.5007652. arXiv: 1709.01980. URL: http://arxiv.org/abs/1709.01980%20http://dx.doi.org/10.1063/1.5007652.

List of Figures

List of Tables